JGR Space Physics

RESEARCH ARTICLE
10.1029/2024JA032458

Comparing Influences of Solar Wind, ULF Waves, and Substorms on 20 eV–2 MeV Electron Flux (RBSP) Using ARMAX Models

L. E. Simms[1,2], **N. Y. Ganushkina**[1,3], **and S. Dubyagin**[3]

[1]University of Michigan, Ann Arbor, MN, USA, [2]Department of Physics, Augsburg University, Minneapolis, MN, USA, [3]Finnish Meteorological Institute, Helsinki, Finland

Key Points:

- Substorms are the predominant driver of eV and MeV electron flux, with less influence on keV flux
- Ultralow frequency waves also influence MeV electrons
- Electrons correlate with input variables even in ARMAX models that correct for autocorrelation and cycling

Correspondence to:
L. E. Simms,
laurasim@umich.edu

Citation:
Simms, L. E., Ganushkina, N. Y., & Dubyagin, S. (2024). Comparing influences of solar wind, ULF waves, and substorms on 20 eV–2 MeV electron flux (RBSP) using ARMAX models. *Journal of Geophysical Research: Space Physics*, *129*, e2024JA032458. https://doi.org/10.1029/2024JA032458

Received 16 JAN 2024
Accepted 23 APR 2024

Author Contributions:
Conceptualization: L. E. Simms, N. Y. Ganushkina
Data curation: S. Dubyagin
Formal analysis: L. E. Simms
Funding acquisition: N. Y. Ganushkina
Investigation: L. E. Simms
Methodology: L. E. Simms
Visualization: L. E. Simms
Writing – original draft: L. E. Simms
Writing – review & editing: L. E. Simms, N. Y. Ganushkina

Abstract Electron fluxes (20 eV–2 MeV, RBSP-A satellite) show reasonable simple correlation with a variety of parameters (solar wind, IMF, substorms, ultralow frequency (ULF) waves, geomagnetic indices) over L-shells 2–6. Removing correlation-inflating common cycles and trends (using autoregressive and moving average terms in an ARMAX analysis) results in a 10 times reduction in apparent association between drivers and electron flux, although many are still statistically significant ($p < 0.05$). Corrected influences are highest in the 20 eV–1 keV and 1–2 MeV electrons, more modest in the midrange (2–40 keV). Solar wind velocity and pressure (but not number density), IMF magnitude (with lower influence of B_z), SME (a substorm measure), a ULF wave index, and geomagnetic indices Kp and SymH all show statistically significant associations with electron flux in the corrected individual ARMAX analyses. We postulate that only pressure, ULF waves, and substorms are direct drivers of electron flux and compare their influences in a combined analysis. SME is the strongest influence of these three, mainly in the eV and MeV electrons. ULF is most influential on the MeV electrons. Pressure shows a smaller positive influence and some indication of either magnetopause shadowing or simply compression on the eV electrons. While strictly predictive models may improve forecasting ability by including indirect driver and proxy parameters, and while these models may be made more parsimonious by choosing not to explicitly model time series behavior, our present analyses include time series variables in order to draw valid conclusions about the physical influences of exogenous parameters.

Plain Language Summary High levels of satellite-damaging electrons (both high and low energy) in the radiation belts appear to be driven by substorms and ultralow frequency waves. There is a positive association between these variables and electron levels even when the cycling behavior of satellite-derived data is corrected. Solar wind pressure, thought to reduce electron levels either temporarily (by compressing the magnetosphere below the level of the nominal L-shell) or permanently (via magnetopause shadowing), shows only a small influence on lower energy electrons. Other solar wind and magnetosphere parameters do show correlations with electron levels even if autocorrelation and cycling behavior is accounted for, but these are not postulated to be direct drivers.

1. Introduction

High levels of electrons in the radiation belts can damage satellites by internal charging (≥100 keV electrons) (e.g., Lam et al., 2012; Loto'aniu et al., 2015) or surface charging (~10–50 keV range) (Thomsen et al., 2013). While the higher energy (>100 keV) electrons generally follow geomagnetic storms, the same is not true of the 10–50 keV electrons which may occur after even moderate substorm activity (Ganushkina et al., 2021; Matéo-Vélez et al., 2018).

A number of parameters correlate with ~2 MeV electron flux at geosynchronous orbit in the radiation belts. These include solar wind velocity (V) (Kellerman & Shprits, 2012; Li et al., 2001, 2005; Paulikas & Blake, 1979), and number density (N) (Balikhin et al., 2011; Lyatsky & Khazanov, 2008). However, the influence of these possible drivers on MeV electron flux may not be direct, but mediated by electromagnetic waves (ULF: ultralow frequency and VLF: very low frequency) and by the electron injections of substorms (Simms, Engebretson, & Reeves, 2023; Simms et al., 2014, 2016; Simms, Engebretson, Clilverd, Rodger, Lessard, et al., 2018). Depending on the situation, higher ULF wave activity is thought to both decrease electron flux levels through outward radial diffusion (Katsavrias et al., 2015; Kellerman & Shprits, 2012; Loto'aniu et al., 2010; K. R. Mann et al., 2012; Ozeke et al., 2020; Turner et al., 2012) or enhance levels through inward radial diffusion (Hao et al., 2019; Katsavrias

et al., 2019; I. Mann et al., 2004). ULF and VLF waves appear to act in tandem, both additively (Katsavrias et al., 2019; Li et al., 2005; O'Brien & McPherron, 2003; Simms, Engebretson, Clilverd, Rodger, Lessard, et al., 2018, Simms, Ganushkina, et al., 2023) and synergistically, with the presence of one wave type enhancing the effect of the other (Simms et al., 2021). However, we use only ULF waves in the present study because high quality VLF data was not available. Pressure, and therefore both velocity and number density, can also lead to flux reductions due to magnetopause shadowing (Shprits et al., 2006; Loto'aniu et al., 2010; Staples et al., 2022; Tu et al., 2019). Substorms may inject seed electrons (hundreds of keV electrons which can be accelerated to high energies) (Birn et al., 1997; Hwang et al., 2007), as well as source electrons (tens of keV electrons that produce VLF waves (Boyd et al., 2014; Friedel et al., 2002; Jaynes et al., 2015; Summers et al., 2002). Southward IMF B_z may correlate with electron enhancements, although this may be through substorm activity triggered by a strongly negative B_z ((Jaynes et al., 2015). Geomagnetic indices (e.g., Kp, SymH, and Dst) also correlate well with flux (Borovsky & Denton, 2014; Lam, 2004; Sakaguchi et al., 2015; Su et al., 2014). Although theory has been proposed that Kp-binned statistical parameterization of solar wind inputs can be used to quantify the accelerating and loss-associated radial diffusion (Lejosne, 2020), the proposed physical action of these indices is not clear. Their high correlation with parameters listed above may mean that they are not drivers but correlates of the drivers.

However, the correlations of lower energy electrons (keV and eV) with various parameters are less well studied. At geosynchronous orbit, responses of keV electrons to solar wind pressure (P) (Shi et al., 2009), velocity (Kellerman & Shprits, 2012; Li et al., 2005), and/or density (Hartley et al., 2014) (30–600 keV) have been found, although Sillanpää et al. (2017) concluded most of the response of 40–150 keV electrons was to solar wind velocity and IMF B_z with less importance attributed to solar wind density, temperature, and pressure (in line with the findings of Li et al. (2005); Kellerman and Shprits (2012); Ganushkina et al. (2019)). Kp and $-V_{SW}B_z$ were successfully used to model 1 eV–40 keV fluxes, suggesting that there are reasonable correlations with these parameters as well (Denton et al., 2016). However, keV fluxes were better modeled using the AE/AL (Auroral Electrojet/Auroral Lower) indices (a measure of substorm activity), together with solar wind speed, than by IMF B_z, Kp, or solar wind number density (Ganushkina et al., 2021). A similar substorm index, SME (SuperMAG electrojet), was also found to be the highest correlate with 40–150 keV flux with solar wind pressure a negative influence (Simms, Ganushkina, et al., 2022). Specifically in the plasmasheet (over a broader L-shell range of L-shell 6–12), keV electrons correlate best with southward IMF B_z (B_s) (Dubyagin et al., 2016), or, more commonly, with solar wind speed combined with B_s (Luo et al., 2011), or the convectional electric field (Stepanov et al., 2021), or *VBs* and IMF B_z (Swiger et al., 2022).

It is often not clear if these correlations are evidence that these factors actually drive increases in electron flux. With time series data, although correlations may contain evidence of physical associations, these can be swamped by the correlation due to cycles and trends that are common to both variables. In addition, autocorrelation in the response variable (electron flux) can increase the apparent statistical significance of correlations. ARMAX models (autoregressive, moving average transfer functions) can address both these problems and are a better choice for analyzing the associations between time series variables (Balikhin et al., 2011; Boynton et al., 2011, 2013, 2015; Sakaguchi et al., 2015; Simms, Engebretson, & Reeves, 2022; Simms, Engebretson, & Reeves, 2023; Simms et al., 2019; Simms, Ganushkina, et al., 2022). The time series behavior of the response variable can be partitioned out by the use of AR (autoregressive) and MA (moving average terms of the error). When chosen well, these AR and MA terms reduce the autocorrelation in the errors of the model and fully describe the cycling behavior of the series. What is left is the association between the response and the predictor variable (the transfer function variable, X) with many of the non-causal correlations removed (Hyndman & Athanasopoulos, 2018). The remaining variability in the data can be tested for its response to external factors (the independent variables). What we will be left with is closer to the actual relationship between the predictor and flux. Note that while we can remove cycles and autocorrelation, it may never be possible to remove all non-causal correlation due to the nature of space weather data. As we are unable to randomly assign "treatments" of, for example, higher or lower solar wind variables, we may never know if there are unmeasured parameters correlated with flux that are the true drivers.

The relationship between electron flux and its possible influences may be nonlinear (Balikhin et al., 2011; Simms, Engebretson, Clilverd, Rodger, & Reeves, 2018). It is often assumed, therefore, that linear models (correlation, regression, etc.) will miss the nonlinear associations, but this apparent difficulty is easily circumvented by transforming the data. Taking the log of the dependent variable (flux) does not remove the nonlinearity, but

describes it in another form. Regressing using the log of only the dependent variable (flux) results in an exponential model. If both dependent and independent variables are logged, the least squares "linear" algorithm of correlation and regression describes a power relation (Neter et al., 1990). Strongly parabolic relationships may be better described by adding a quadratic term to the linear model, but the nonlinearity in the electron flux relationship to its possible drivers is usually adequately described by an exponential model derived from the log transformation.

Using ARMAX models, we have previously explored the influence of parameters on hourly averaged geosynchronous orbit (L-shell 6.6) 40–150 keV and 1.8–3.5 MeV electron flux (Simms, Engebretson, & Reeves, 2022; Simms, Engebretson, & Reeves, 2023; Simms, Ganushkina, et al., 2022) (GOES and LANL satellites). In the present paper, using 10 min averaged electron flux data from the van Allen probes (RBSP: Radiation Belt Storm Probes), we expand our investigation to include more L-shells (L-shell 2-L-shell 7) and a wider range of energies (20 eV–2 MeV). Although previous work has explored the influence of waves on higher energy (>1.5 MeV) electrons at different L-shells (Simms et al., 2021), and solar wind and IMF parameters on lower energy electrons in the plasmasheet at ≥L-shell 6 (Dubyagin et al., 2016; Luo et al., 2011; Stepanov et al., 2021; Swiger et al., 2022), there is less information about lower energy electrons below geosynchronous orbit. Expanding the analysis to further L-shells will improve our understanding of the radiation belt electron dynamics, but this complicates the analysis as L-shell is now another factor that must be accounted for. We address this by entering L as a categorical variable which is then used to separate out the effects at each L. As with previous work on geosynchronous electrons, we also use magnetic local time (MLT) as a covariate to account for variability associated with location.

We postulate that the main direct drivers of electron flux changes are substorm injection of electrons, processes driven by waves such as radial diffusion, and compression and subsequent magnetopause shadowing due to solar wind pressure. While other parameters may correlate highly with electron flux, few mechanisms have been proposed whereby these other variables might physically drive flux changes. To determine the relative contributions of each of these three direct driver processes, we analyze them in combination so that effect of each can be measured with the others held constant.

2. Data and Statistical Analyses

The Van Allen Probes mission (Mauk et al., 2013), designed for studies of Earth's radiation belts, was launched in August 2012 and operated until October 2019. It consisted of two spacecraft in elliptical orbits around Earth, traversing the inner magnetosphere at distances from 1.1 RE to 5.8 RE at a near-equatorial (10°) inclination and a 9-hr period. The two satellites had slightly different orbits, with one lapping the other every ∼2.5 months. Data are from REPT (Relativistic Electron-Proton Telescope) (Baker et al., 2012), the HOPE (Helium Oxygen Proton Electron) instrument (Funsten et al., 2013), part of the thermal plasma (Radiation Belt Storm Probes ECT) suite (Spence et al., 2013), which measured the pitch angle distribution of electrons over the energy range from 30 eV up to ∼45 keV, and the Magnetic Electron Ion Spectrometer (MagEIS) instrument (Blake et al., 2013) which used magnetic focusing and pulse height analysis to provide the energetic electron measurements over the energy range of 20 keV–4 MeV. Although this data set is mostly focused on pitch-angle resolved data, the.cdf files also contain the omnidirectional flux spectra (FEDO variable, see Supporting Information to Boyd et al. (2021)). We use these spectra (3 min averaged) in the 20 eV−2 MeV energy range, and subsequently average them to 10 min for the ARMAX analyses and 1 hr for the correlation analyses. We used the data for only one probe (RBSP-A) over 1 Feb 2013–31 Dec 2018 over L-shell 2-L-shell 7 (although little time is spent in L-shell 7). Data are binned by McIlwain L shell values, with, for example, $L = 2$ containing all values $L = 2.00$–2.99. These data are available at: https://rbsp-ect.newmexicoconsortium.org/datapub/rbspa/ECT/level3/ from the main page at: https://rbsp-ect.newmexicoconsortium.org/science/DataDirectories.php.

Solar wind and IMF parameters as well as geomagnetic indices (Kp index and SymH), were obtained from OMNIWeb with data time-shifted to the bow shock nose: https://omniweb.gsfc.nasa.gov/form/dx1.html.

These 5 min averages were then averaged to 10 min for the ARMAX analyses and to 1 hr for the correlation analyses. In addition to the Kp and SymH indices, these variables consisted of solar wind velocity (V), number density (N), pressure (P), IMF B, B_y, and B_z (all GSM), and the f10.7 solar flux (Solar). We use the SuperMAG (https://supermag.jhuapl.edu/) SME index (SuperMAG electrojet index) as a proxy for substorm activity and their hypothesized injections of lower energy electrons (Gjerloev, 2012; Newell & Gjerloev, 2011). Although the

darkside SME (SMEd: an SME index using only data collected from darkside magnetometers) might be expected to pick up more of the substorm signal, we were unable to use this in the ARMAX models due to larger and more frequent data gaps. The hourly ULF index was obtained from http://ulf.gcras.ru/archive.html (Kozyreva et al., 2007; Romanova & Pilipenko, 2009).

Statistical analyses were performed in MATLAB (The MathWorks Inc., 2023).

To reduce heteroscedasticity and nonnormality of the resulting residuals from these analyses, and therefore to make inferences more robust, all wholly positive parameters and Kp + 1 were logged, following the averaging to 10 min (see above). This has the added benefit of linearizing the relationship between electron flux and predictors, justifying the use of linear models such as correlation, regression, and ARMAX methods. Note that this does not remove the nonlinearity, but merely describes it in another form. In effect, the models are now power relationships (if both flux and predictor are logged) or exponential relationships (if only flux is logged). Residual analysis of the errors of these models on transformed data showed random errors with no suggestion of further nonlinearity. Thus, the nonlinear relationships previously noted between electron flux and possible predictors (e.g., Simms, Engebretson, Clilverd, Rodger, & Reeves, 2018; Balikhin et al., 2011) are not intrinsically nonlinear and can be easily analyzed with linear models such as correlation or regression if the data are first transformed (Neter et al., 1990).

To produce unitless, and therefore directly comparable ARMAX regression coefficients, we calculated the Z scores: subtracting the mean of each variable and dividing by the standard deviation for all observations. For the simple correlations, the input parameters were averaged hourly, with electron flux at each energy averaged over both hour and L-shell 2–7, although there were a much lower number of observations in L-shell 7.

Correlation and ARMAX coefficients are labeled statistically significant if their p-value, the probability that the null hypothesis of zero effect is being falsely rejected, falls below the generally accepted 0.05 level. These p-values are calculated assuming a normal distribution, taking into account the strength of the apparent relationship, the variance, and the sample size. The standard formulas for calculating the p-values in linear models are reported by the MATLAB statistical package and are available in standard statistical texts (Neter et al., 1990). On the figures, the range of values for which correlation and ARMAX coefficients are statistically nonsignificant ($p > 0.05$) is identified by a gray bar.

We perform two types of analysis: simple correlations with predictor variables measured every 10 min over the 48 hr prior to the electron flux observation, and ARMAX regression models for every 10 min over the 6 hr before the flux observation. Simple correlations were performed between each parameter and each flux energy averaged over each L-shell. L-shell was assigned to L-shell 2 if L-shell was 2.00–2.99, etc. However, these correlations include not only the association between each parameter and flux but also, potentially, autocorrelation in the response variable and any common trends or cycles that are not related to the physical relationship. For this reason, we cannot depend on single correlations to determine which are the driving parameters of electron flux. We must use ARMAX models to describe the time behavior of the response variable (electron flux). We introduce AR and MA terms to specifically describe the cycling and autocorrelation (where a variable is correlated with itself at different times) that may be present in time series data. These terms include autoregressive components (regressing on previous values of the dependent variable: an AR term), or a moving average component (regressing on the errors of the model at preceding time steps: an MA term). "Seasonal cycles" (at a set time period) may also be fit with seasonal AR and MA terms. If "seasonal" effects and autocorrelation have been sufficiently removed, the partial autocorrelation function (PACF) of the residuals of the model will show no peaks. The PACF gives the partial correlations of the time series with itself at its own lagged values (Hyndman & Athanasopoulos, 2018).

For our ARMAX models, data were averaged to 10 min intervals, with L-shell categorized as the most common L-shell in that period. In most cases, this was a single L-shell. Gaps were filled using linear interpolation between neighboring points before logs were taken. Data already at a ≥1 hr cadence (the ULF index, Kp, solar f10.7) were left unchanged. An AR1/MA2 (autoregressive term at 1 time step, moving average term at time steps 1 and 2) model removed some of the autocorrelation in the residuals, but we found that adding "seasonal" AR and MA terms (SAR1 and SMA1: additional autoregressive and moving average terms both at the "seasonal" 9 hr lag, the period of the satellite) provided more improvement (Figure 1). In Figures 1a and 1b, the autocorrelation of the residuals are high in models uncorrected for time series behavior at both the lowest (50 eV) and highest (2 MeV)

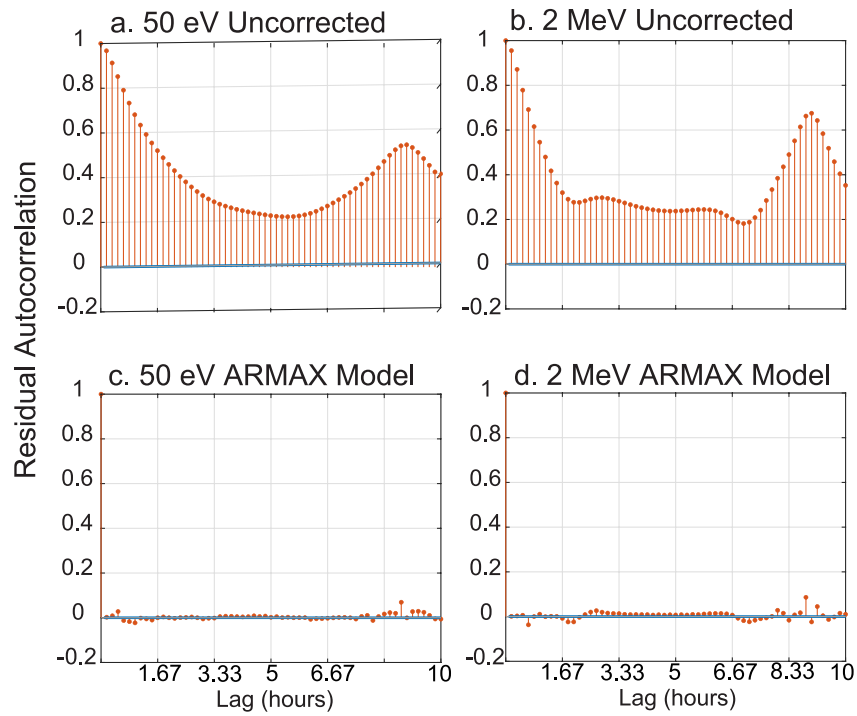

Figure 1. Autocorrelations of the residuals for regression models without correction (a and b) and for models with AR and MA terms describing time series behavior of electron flux (c and d) for 2 energies (50 eV and 2 MeV). The high autocorrelation in the residuals in a and b show that ARMA correction is needed, while the much lower autocorrelations of c and d show that the ARMA terms describing time series behavior have succeeded in removing most autocorrelation and the 9 hr cycling behavior due to the satellite orbit.

electron energies. However, in Figures 1c and 1d, the autocorrelation has been mostly removed by the introduction of AR1, MA2, SAR1, and SMA1 terms to the analysis. Although differencing, subtracting a previous observation from the current observation at a set time step, is often helpful in removing cycling behavior, we found that differencing electron flux at 9 hr (subtracting the observation from 9 hr previous) introduced a strong negative autocorrelation at 9 hr (not shown).

ARMAX models were fit using the ordinary least squares method. For each predictor, a separate model was fit at each 10 min time step over 6 hr resulting in 36 models for each parameter. Individual models used only a single exogenous parameter at a time. Combined ARMAX models using P, ULF, and SME as simultaneous predictors were also fit at every 10 min over 6 hr.

We add MLT as a covariate to control for varying levels of electron flux around the Earth. This was entered as two variables, $\sin(2\pi \times MLT/24)$ and $\cos(2\pi \times MLT/24)$, however, this made little difference in the overall influences of parameters.

Although solar flux can be used to find daily and hourly correlations, it becomes less useful in the 10 min ARMAX analyses as the value changes only daily, at most. Kp also changes at a slower cadence (3 hr), although this is fast enough to result in some response.

We are most interested in (a) the determination of statistical significance, that is, the ability to reject the hypothesis that there is no relationship between variables, (b) how much each statistically significant parameter influences flux in comparison to the others, and (c) determining the influence of each parameter independent of correlation-inflating cycles and trends:

1. Statistical significance is reported as a *p*-value: the probability that a null hypothesis is true. This type of inference test determines the probability that associations between variables are due only to chance. When a *p*-value is below 0.05, we feel confident in rejecting the null hypothesis and accepting that there is an association between variables and a possible influence. *P*-values were determined using the standard error at 71 keV at

Table 1
Means and Standard Deviations for Conversion of log_{10} Electron Flux to Z-Scores

	Mean	Std Dev
20 eV	732685690.5	622843189.7
50 eV	121447923.3	130175086.7
1 keV	42082599.62	47864441.26
2 keV	18835776.85	25596479.18
4 keV	9705617.529	13837821.32
6 keV	6455566.093	10197659
11 keV	4135913.188	7397497.773
18 keV	3142601.156	5968156.437
32 keV	2106425.54	4241707.493
40 keV	1708448.914	3551010.212
71 keV	921662.4553	1980250.368
100 keV	615382.1619	1276947.064
158 keV	209529.03	351649.8774
1 MeV	28803.91726	39026.83643
2 MeV	8510.835041	14849.23535

hour 3 at each L-shell as this showed the most variation, however, the critical p-value cut off was almost identical for all energies. In Figures 2–7, we show nonsignificant results (p-value >0.05) between gray bands. Because the satellite spent much less time at L-shell 7, resulting in fewer degrees of freedom, and because the variability in this region was higher, the band of nonsignificance is higher for this region (Neter et al., 1990). We therefore put less stock in the results from this L-shell, but we were not able to remove L-shell 7 from the ARMAX models as a continuous time series is needed for these analyses. Additionally, entering L-shell as a covariate not only allows us to determine the effect of a predictor at each L-shell and at each time lag, but has the added advantage of increasing sample size which raises the power of the statistical test and lowers the likelihood of missing significant relationships.

2. The contribution of each parameter to electron flux values cannot be directly compared if the units vary. In order to make these comparisons, we perform a Z score transformation (see above) to standardize to a common standard deviation. These unitless coefficients can be transformed back to the original units with the means and standard deviations if comparisons to other studies are desired (Table 1). In essence, the standardization to a common standard deviation replicates the ability to compare correlation coefficients across input parameters of varying units. As correlations are unitless, correlations of Z score transformed data will be the same as with untransformed data.
3. Correlations from studies that do not account for the problem of autocorrelation in the time series will be composed mostly of common cycles and trends, therefore we must remove autocorrelation and cycles by the use of ARMAX regression. The ARMAX coefficients we find are much lower than correlation coefficients, as the spurious correlations due to cycles and autocorrelation have been removed, but they are more accurate representations of the relationships of interest. In the ARMAX models, L-shell is entered as a categorical variable for ease of presentation. These are coded as indicator ("dummy") variables, with additional multiplicative interaction terms created between these 0,1 variables and each predictor. Coefficients at L-shell 2 are then read directly while coefficients from each other L-shell are calculated by adding their specific interaction term to the L-shell 2 "base" coefficient. This allows a graphical presentation of coefficients by L-shell.

3. Simple Correlations

Pearson correlations, often termed "simple" correlations because each analysis contains only two variables, are performed over 48 hr for just the lower energy flux (20 eV–6 keV) with each parameter. These show reasonably high, statistically significant influences of V, P, B, B_z, SME, ULF, and SymH (Figure 2), similar to what has previously been found for 11 keV–2 MeV flux (Simms, Ganushkina, et al., 2022; Simms, Ganushkina, et al., 2023). Nonsignificant correlations (where $p > 0.05$) lie within the gray areas. The correlation with N is lower, and B_y shows little correlation. These influences often appear strongest at L-shells 4–6. While we show the results at L-shell 7, these are less reliable because of the low sample size.

As a comparison to the ARMAX coefficients (below) over a wider range of energies, we correlate 3 flux energies (50 eV, 18 keV, 2 MeV) with each predictor measured 3 hr previous ("Lag 3") at 3 L-shells and with two additional variables (Kp, and solar flux). Previous work found that the Lag 3 (hour) correlations were very similar to the Lag 0 and Lag 1 hr correlations at GOES over 40 keV–2 MeV (Simms, Ganushkina, et al., 2022; Simms, Ganushkina, et al., 2023). However, we choose Lag 3 here to avoid the possibility that the predictor measurements may occur before the flux measurement, given that solar wind variables are measured upstream. Correlations of each parameter with flux show reasonably high (up to 0.5), statistically significant influences of V, B, B_z, SME, ULF, Kp, and SymH (Figure 3). The correlations of electron flux with P, N, B_y, and solar flux are lower.

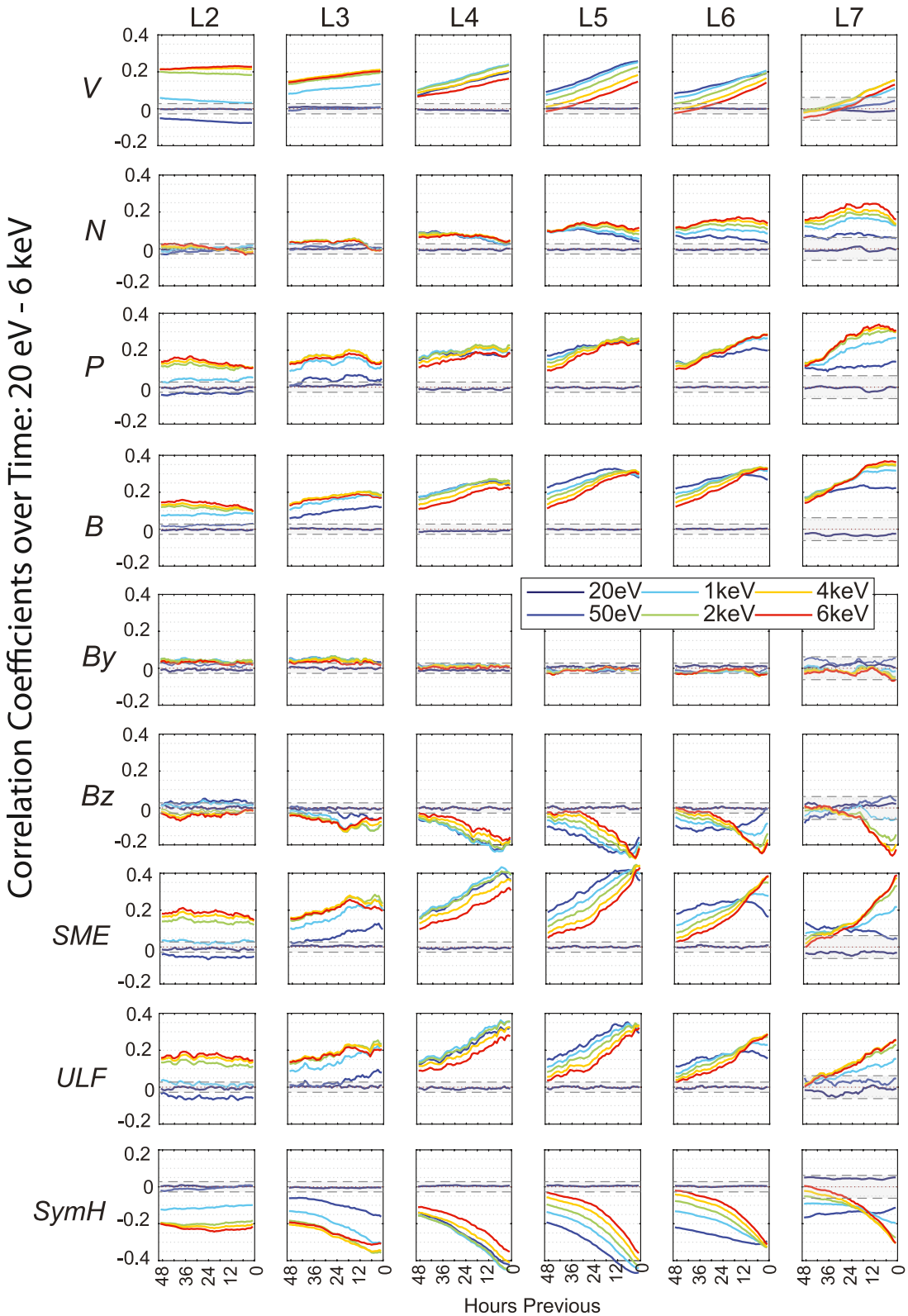

Figure 2. Simple correlations of low energy electron flux (20 eV–6 keV) with V, N, P, B, B_y, B_z, SME, ULF, and SymH over 48 hr. These simple correlations, uncorrected for autocorrelation and cycles, are as high as 0.45. Nonsignificant correlations ($p > 0.05$) lie within the gray area.

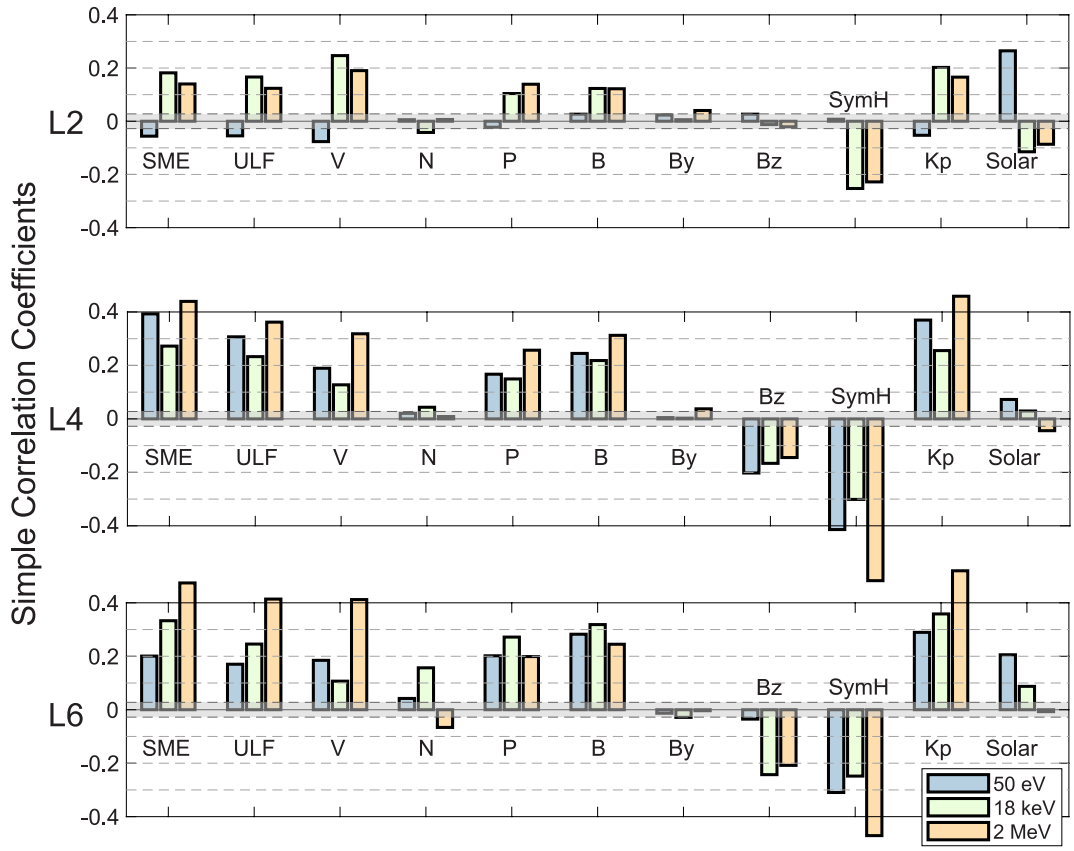

Figure 3. Simple correlations of V, N, P, B, B_y, B_z, SME, ULF, Kp, SymH, and solar flux with electron flux at Lag 3 hr prior to the electron flux observation (50 eV, 18 keV, and 2 MeV flux, at L2, 4, and 6). These simple correlations, uncorrected for autocorrelation and cycles, are as high as 0.45. Nonsignificant correlations ($p > 0.05$) lie within the gray area.

4. ARMAX Analyses: Individual Parameters

If the time behavior of electron flux is modeled separately using AR and MA terms, the remaining variation associated with solar wind, IMF, ULF wave, and geomagnetic influences on electron levels is less than a tenth of what is suggested by simple correlation analysis (Figures 4 and 5). In these figures, we plot the regression coefficient (not the correlation coefficient) for each predictor variable. This is the term that describes the association between predictor and flux once the time behavior has been removed via the AR and MA terms. As each 10 min time step and electron energy is analyzed separately. The terms in these ARMAX models include 1. L-shell as a categorical variable, 2. MLT as an explanatory covariate, 3. the AR and MA terms used to model time series behavior, and 4. the predictor variable at that point in time (Lag x). Only the coefficients associated with the predictor variable at Lag x are shown in the figures. Coding L-shell as a categorical variable allows us to determine the effect of a predictor at each L-shell and at each time lag, while still being able to use all the data in a single analysis, as required by ARMAX models, instead of breaking it into smaller subsets.

As we use Z scores, these ARMAX coefficients are directly comparable between the simple correlations and the ARMAX analyses. Consequently, we have demonstrated that the simple correlations are greatly inflated by the cycles in the various time series. The advantage of the ARMAX approach is that we are able to test whether there is any significant association between electron flux and parameters independent of common cycles and autocorrelation. We do find statistically significant effects, even if they are lower than we might initially expect based on the simple correlations.

There is a shift in the relative response of flux over L-shells. In contrast to the higher response at L-shell 4 and 6 in the simple correlations, we now also see more response in the lower L-shells for most of the parameters. However,

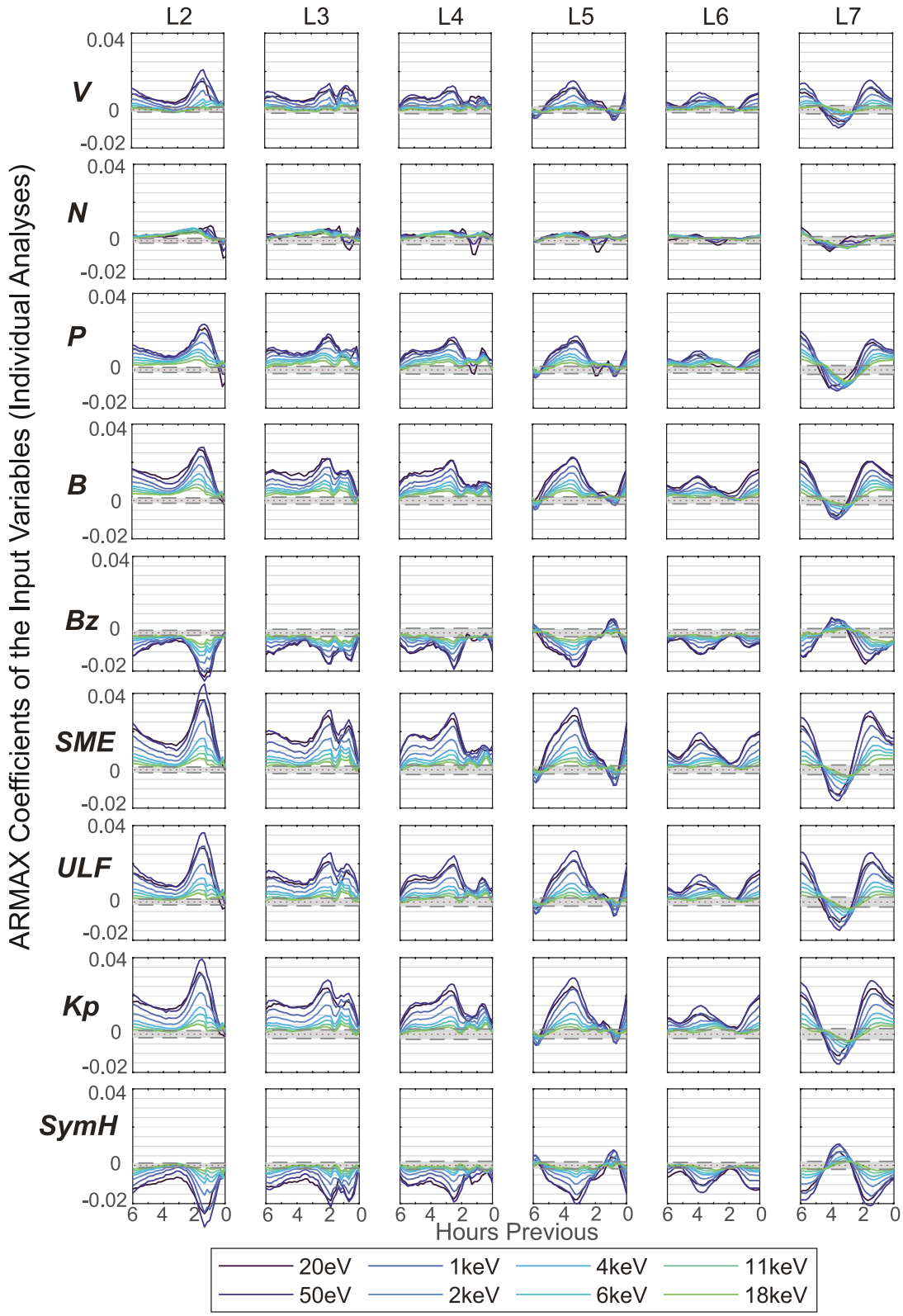

Figure 4. Coefficients from a series of ARMAX models using each exogenous variable individually over 20 eV–18 keV electron flux (Z scores). Each point is the regression coefficient for that variable at each 10 min interval over 6 hr prior to the electron flux measurement. This is similar to a cross correlation plot except these influences are corrected for autocorrelation and cycles using AR and MA terms (not shown). Coefficients peak at ~0.04, ten times less than simple correlations. However many are still statistically significant, lying outside the gray nonsignificant ($p > 0.05$) region.

N still shows little association with electron flux. The strongest influence is often at about 1–2 hr at L-shell 2–3, at 3–4 hr at L-shell 4, and at 4–6 hr at L-shell 5. Again, the results at L-shell 7 are less reliable due to the very small sample size in that L-shell. We do not show the ARMAX models for B_y and solar flux because B_y shows little simple correlation with electron flux and solar flux does not change over 24 hr.

Kp and SymH show strong apparent influence. However, Kp, at a 3 hr cadence, is less likely to give us much information on the more rapid flux changes, and neither Kp nor SymH has been postulated to represent a physical process that drives electrons. Instead, they have often been used in modeling as they are a strong correlate and/or a proxy of other processes that have either not been measured or are more conveniently represented by a single number.

5. ARMAX Analyses: Combined Parameters

We combine P, SME, and ULF, as the three possible direct drivers, into one ARMAX model for each energy (Figures 6 and 7). At low energies, SME shows the most association with flux, with the highest response at L-shell 2 and roughly equal response over L-shell 3–6. ULF is the dominant influence at the higher energies (1–2 MeV), with roughly equal effect over L-shell 2–5 and no indication of electron losses due to ULF waves. Both SME and ULF appear to have more immediate influence at L-shell 2–3 (1–2 hr), a more delayed response at higher L (3–4 hr), and an even more immediate response appears at L-shell 6 (0–1 hr).

The responses to SME and ULF are no longer as suspiciously similar as they were in the individual analyses. The intercorrelation of these three variables means their similar associations with flux are not diagnostic of their similar influences but only of their similar response to other variables in the IMF and solar wind. However, by combining them in the same ARMAX analysis, we are able to look individually at the effect of each independent of the others.

There is less influence of P when both SME and ULF are accounted for. It is mostly a positive influence. There is a short negative effect on the lowest energy (20 eV) within the first 2 hr, but there is not strong evidence of magnetopause shadowing following compression at other energies and this negative influence may simply be the result of compression below the nominal L-shell.

6. Discussion

Previous cross correlation analyses on 40 keV - 2 MeV electrons at geosynchronous orbit showed high correlations between flux and possible drivers over a 48 hr period, although the removal of trends and cycles using ARMAX analysis reveals the associations occur within only a few hours of the flux measurement (Simms, Ganushkina, et al., 2022; Simms, Ganushkina, et al., 2023). The precise timing of action (i.e., at what lag each variable is most influential) is obscured by the high correlation of each parameter with itself over time. Because of this autocorrelation within each predictor, it would be incorrect to attribute a long term influence to them even though high correlations occur over a number of hours. In addition, autocorrelation, as well as common cycles and trends, can result in spurious associations between variables. Removing these using the ARMAX methodology results in associations at least an order of magnitude lower, meaning that the simple correlations are almost entirely showing the larger influence of autocorrelation and common cycling, not any driving behavior. However, with autocorrelation and cycling removed, we are now able to detect associations of electron flux with V, P, B, B_z, SME, ULF, Kp, and SymH over the 6 hr prior to the flux observation. N was rarely statistically significant. These responses were stronger in the higher (1–2 MeV) and lower (20 eV–1 keV) electrons than in the mid-range energies. Previously, 40–150 keV electrons at geosynchronous orbit were found to show a negative response to P and a smaller positive response to both the AE index (auroral electrojet. also measured by SME) and ULF, when these variables (lagged by 1 hr) were analyzed independently (Simms, Ganushkina, et al., 2022). In the present study, expanded spatially (L-shell 2–L-shell 6), temporally (over at least 6 hr), and over a wider range of electron energies (20 eV–2 MeV), we find similar responses in the keV range. However, the influences on both eV and MeV electrons are somewhat stronger.

There are several variables we do not analyze with ARMAX models: B_y showed trivial associations in the simple correlations and solar flux does not change quickly enough to study the more rapid changes in electron flux. In addition, although Kp and SymH show associations as strong as other variables, we do not consider them possible

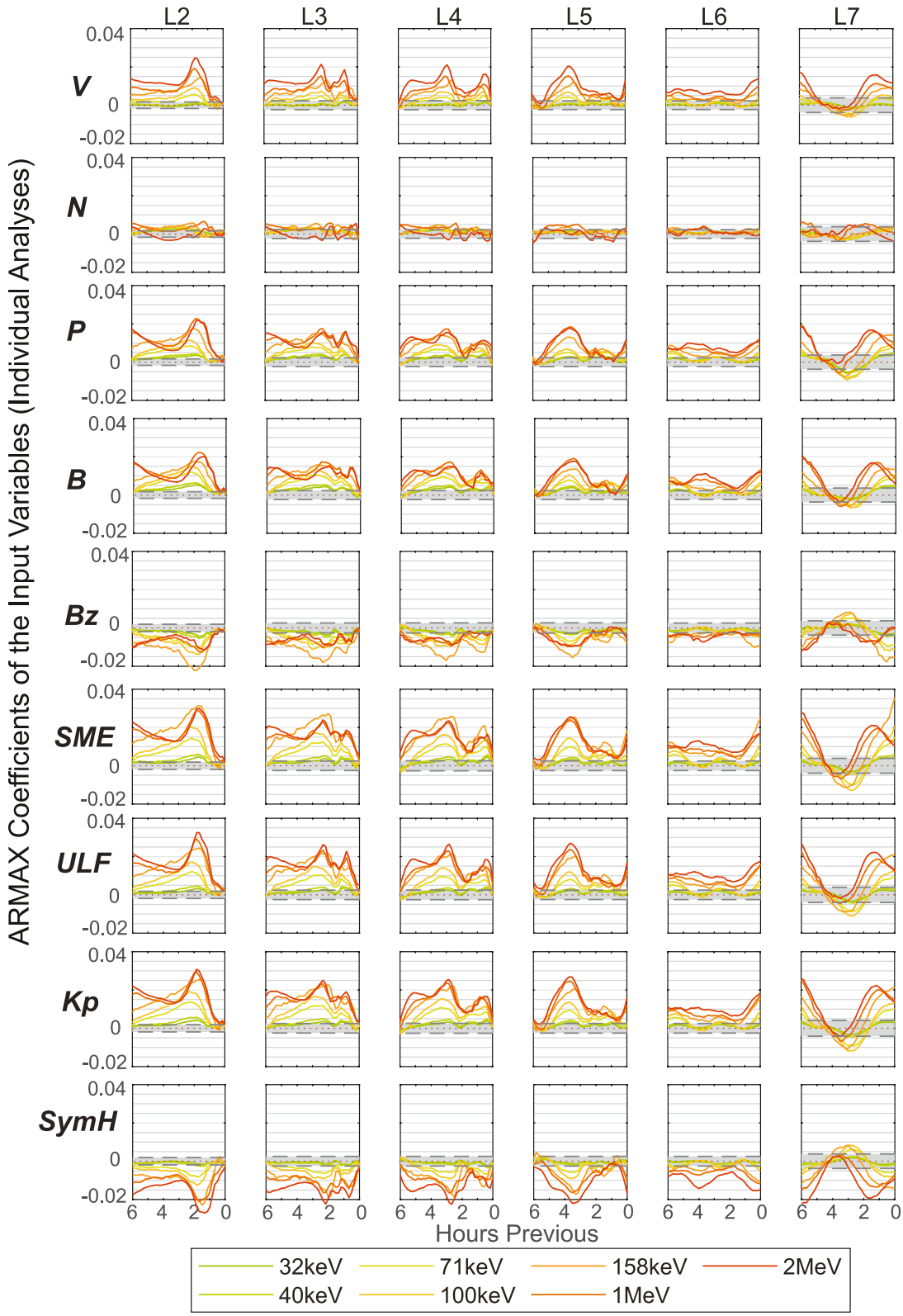

Figure 5. Coefficients from a series of ARMAX models using each exogenous variable individually over 32 keV–2 MeV electron flux (Z scores). Each point is the regression coefficient for that variable at each 10 min interval over 6 hr prior to the electron flux measurement. This is similar to a cross correlation plot except these influences are corrected for autocorrelation and cycles using AR and MA terms (not shown). Coefficients peak at ~0.03, an order of magnitude below simple correlations. However many are still statistically significant, lying outside the gray nonsignificant ($p > 0.05$) region.

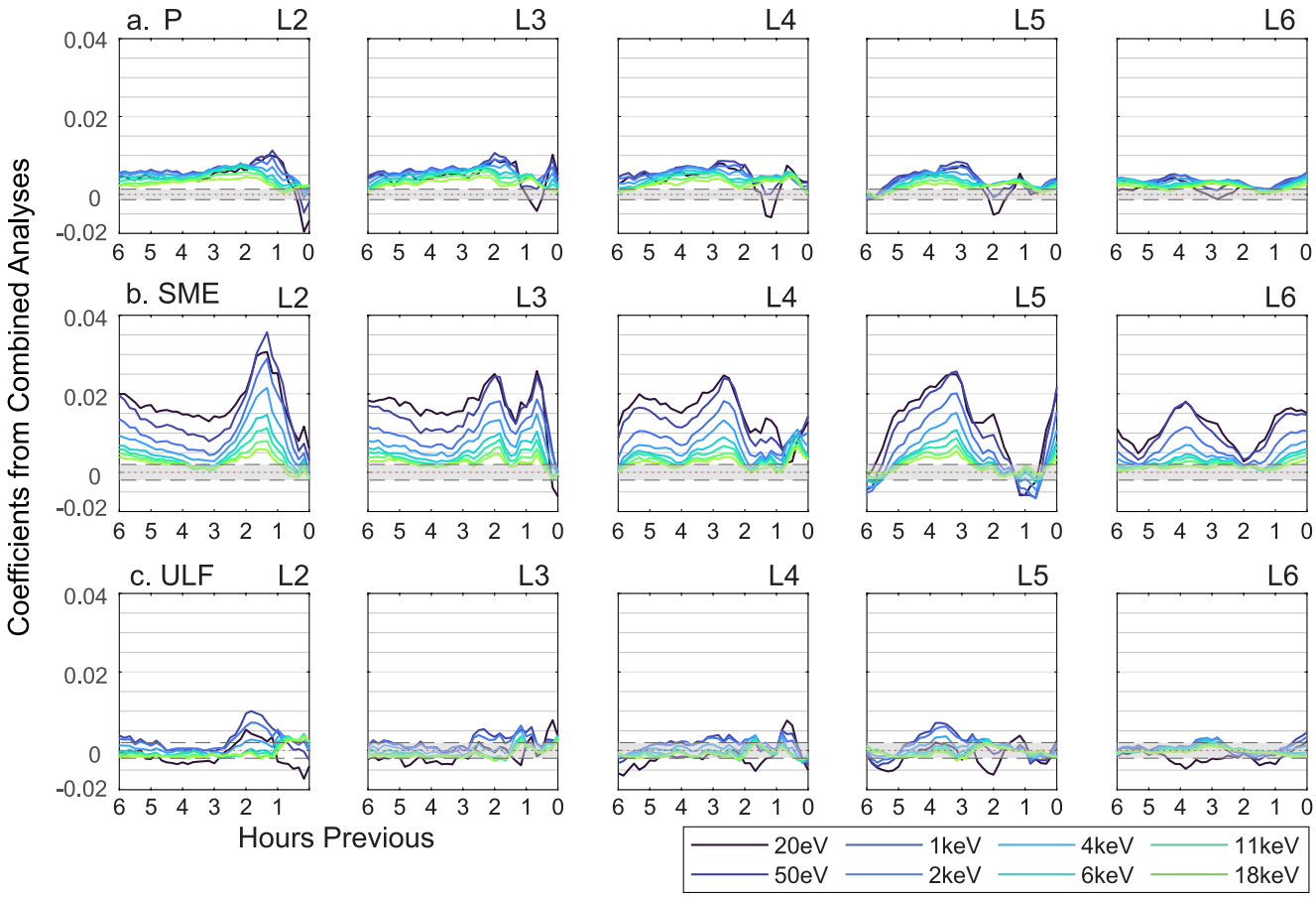

Figure 6. Coefficients from ARMAX models combining the three postulated direct drivers of electron flux: P, SME, and ULF (Z scores) at 20 eV–18 keV.

drivers because they are only generalized measures of geomagnetic activity and not postulated to represent a specific physical process that might be associated with electron flux changes.

In contrast to predictive models, in this study we use statistical tests of inference that test hypotheses about physical drivers. We ask *which* parameters are influential (not just correlated) and *how much* they may influence electron levels. Simple correlations do not answer either of these questions as they are highly contaminated by spurious correlations due to irrelevant cycles and trends. The same is true of more sophisticated machine learning models such as neural networks where coefficients cannot be interpreted as explanatory despite the identification of the most "important" by means such as the Shapley method (e.g., Swiger et al., 2022; Ma et al., 2023). The time series behavior must be removed (Simms, Engebretson, & Reeves, 2022) or described separately using ARMAX modeling in order to identify the underlying physical relationships. This is not to say that ARMAX models cannot be used to build effective prediction models (Balikhin et al., 2011, 2016; Sakaguchi et al., 2013; Sakaguchi et al., 2015; Simms & Engebretson, 2020; Simms, Ganushkina, et al., 2023), and if prediction is the only goal, modeling using such methods as regression, correlation, or neural networks do not need to model time series behavior as a separate influence because the set of variables *as a whole*, exogenous variables plus intrinsic time behavior, can effectively predict flux. The only caveat is that we cannot make the jump to assuming that uncorrected, highly correlated relationships give any information on the physical drivers. As an example, at geosynchronous orbit, statistically significant influences, corrected for time series behavior, in the 4.1–30 keV or 40–75 keV range are often low, but this does not preclude building an adequate prediction model with the time series behavior left embedded in the response variable instead of being separated out into independent terms (Simms, Ganushkina, et al., 2022).

We can class these variables into possible direct drivers (those with a hypothesized physical mechanism that would affect electron flux), indirect drivers (solar wind and IMF inputs that could be expected to influence the

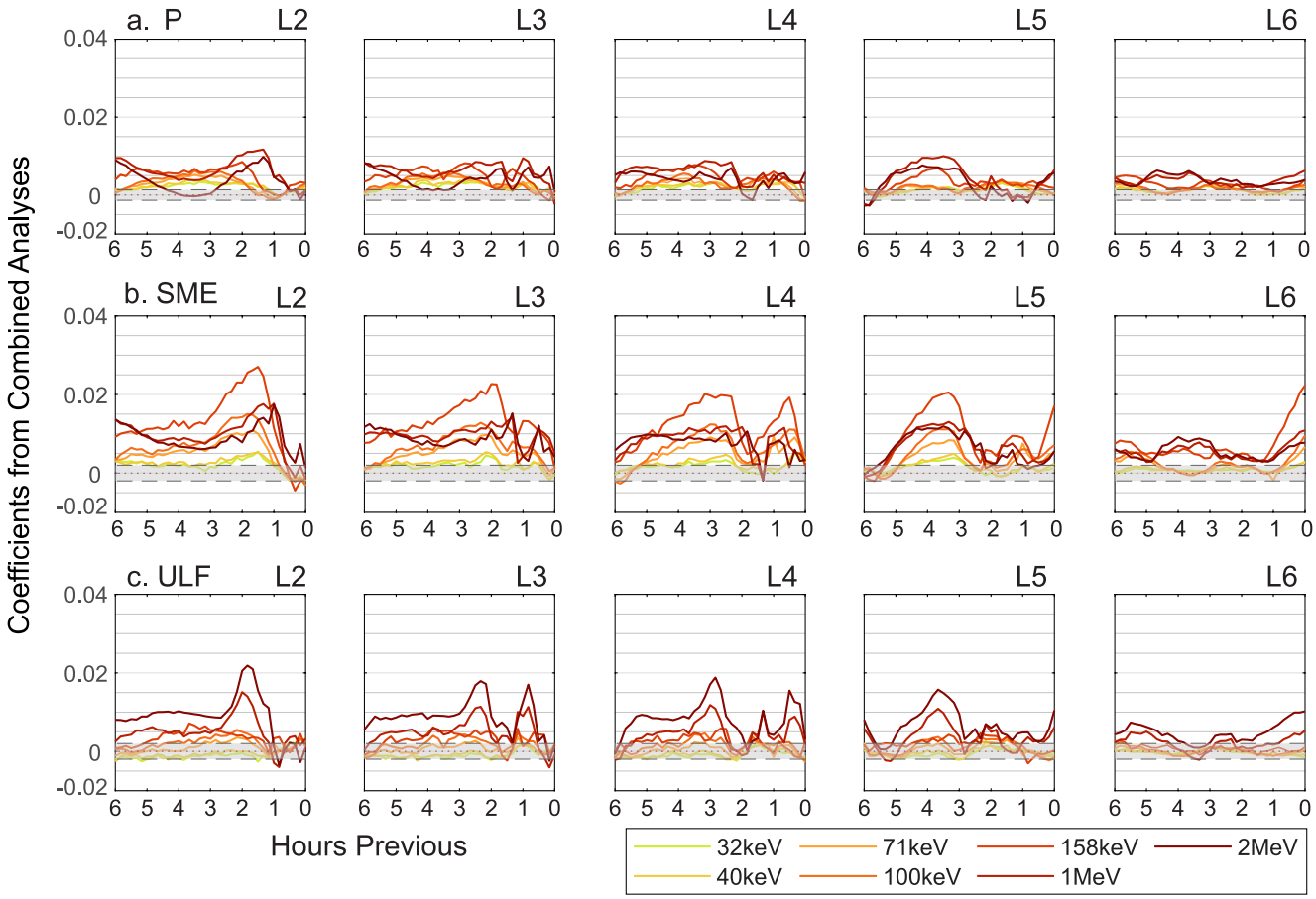

Figure 7. Coefficients from ARMAX models combining the three postulated direct drivers of electron flux: P, SME, and ULF (Z scores) at 32 keV–2 MeV.

direct drivers but do not themselves have a postulated mechanism of influence), and proxy variables (indicators of generalized geomagnetic activity with no postulated mechanism of influence on electrons). In the space weather community, substorms, waves, and solar wind pressure are generally postulated to have a direct influence on electron flux (Simms et al., 2021; Simms, Ganushkina, et al., 2022). Solar wind and IMF influences, while often highly correlated with flux, have not been proposed to have a direct mechanism of influence on electrons but instead on the proposed direct drivers. The exception here is solar wind pressure which may act as a hybrid of direct and indirect influences. The direct component can be the result of magnetosphere compression (magnetopause shadowing) leading to a loss of electrons or simply a temporary constriction of regions below their nominal L-shell. The indirect component of pressure, as with velocity, number density, and the IMF, is through their ability to increase both substorms and waves.

Proxy variables include Kp and SymH, measures of activity that may be a conglomerate of other variables, measuring both the postulated direct influences (e.g., substorms and waves) as well as other unidentified processes. The SME index may straddle the line between proxy (being a general measure of geomagnetic activity) and direct influence (as it measures electron-injecting substorm activity). Although we use it to "measure" substorms, we are aware that it is a problematic variable, likely measuring more processes than we suppose or would like. However, it is the best measure of substorms that we currently have.

In our current study, SME and ULF show such a similar pattern of influence that it suggests they act as proxies for each other. This is not surprising, given that the auroral electrojet indices and ULF indices are highly intercorrelated (Simms et al., 2014), but to determine the actual influence of each they should be combined in a single analysis. In the combined analysis, using P, SME, and ULF as the postulated possible direct drivers, the responses to SME and ULF are no longer as similar as they were in the individual analyses. The confounding correlations due to these variables being correlated with each other are accounted for by analyzing them together, so we can

say with more evidence that SME is more influential than ULF on the lower energy flux and of approximately equal importance in the higher energy ranges. SME showed the most association with low energy flux (20–50 eV). Both ULF and SME showed similar influences on the high energy flux (1–2 MeV), but mid-range flux was not as highly influenced by either of these variables. The positive influence of P is generally lower, and there is a negative influence in the lowest energies, nearly immediate at L-shell 2 (∼0 hr), but moving gradually earlier at higher L (∼2 hr). In the 40–150 keV range, the low response to P and ULF, with a higher response to SME, is in line with what was found previously at geosynchronous orbit (Simms, Ganushkina, et al., 2022).

The possible substorm (SME-measured) injection of low energy (<4 keV) electrons may not be immediate. The largest peak of influence occurs at ∼1–2 hr at L-shell 2, 0.5–2.5 hr at L-shell 3, ∼3 hr at L-shell 4, 0 or ∼4 hr at L-shell 5, and 0–1 and ∼4 hr at L-shell 6. It is unclear why the introduction of low energy electrons into the higher L shells would take more time. An argument could be made that these electrons are first introduced into the loss region and subsequently make their way into the higher L shells, but there is no proposed mechanism for this.

Mid-range electrons do not show this response, and it is possible that the response of high energy electrons may be due to the general geomagnetic disturbance information contained in SME instead of specific substorm activity, as it is not expected for higher energy electrons to be injected.

The ULF influence is seen mostly in the 1–2 MeV range. In previous work, ULF waves have been found to be a stronger influence if only storm recovery time periods are considered (at ∼L-shell 6) as long quiet periods might tend to "wash out" the influence of parameters that are only rarely strong enough to be active (Simms, Engebretson, & Reeves, 2023). For MeV electrons, which rise after geomagnetic storms, it is possible to study just the after-storm response with a reasonable sample size (i.e., more than just one or a few storms) (Simms et al., 2014), but lower energy electrons do not show stronger responses to drivers during storms (Simms, Ganushkina, et al., 2022), so there are no easily identifiable points at which responses can be studied. Therefore, correlations over long periods are the only reasonable way to search for low keV (and, presumably, eV) responses. This positive influence of ULF waves may be evidence of accelerating radial diffusion. One might also expect that there would be visible loss in the lower energy ranges, as a consequence of some subset of them being driven to the higher energies and thus reducing the lower energy population. This might not be noticeable, given the relative sizes of the high and low energy populations, with high energy electrons being fairly low in comparison, but there is some suggestion of this in the 20 eV–1 keV electrons at L-shell 5. We have previously found a suggestion of ULF waves lowering 40 keV electrons during storm recovery, although not the 75–150 kev electrons, at ∼L-shell 6 (geosynchronous orbit) (Simms, Ganushkina, et al., 2022).

The lower influence of ULF waves in the ARMAX models vs the simple correlations cannot be interpreted to mean that radial diffusion due to ULF waves is less important than local acceleration by VLF waves in accelerating MeV electrons (Lejosne, 2020). In fact, it has previously been shown that these two factors act both simultaneously and synergistically, at least at a daily cadence (Simms et al., 2021). However, the lower coefficients we obtain for a ULF influence, corrected for time series autocorrelation and common cycles, have a bearing on what magnitude of coefficients would be appropriate in models of radial diffusion due to ULF waves (Ozeke et al., 2014). Previous high, long-period correlations found between electron flux at geosynchronous orbit (2 MeV) are too contaminated with cycling and autocorrelation to form a basis for determining accurate diffusion coefficients, for example, Borovsky and Denton (2014); Simms et al. (2016).

When time series behavior is removed, the comparatively low response of electrons to the possible drivers (compared to simple correlation coefficients) is not a failure of the analysis, but simply a function of removing the substantial cycling noise and autocorrelation from the effect previously erroneously attributed to the predictor variables. Once this noise is removed, variables may be deemed important or not based on whether they are statistically significant and by comparing to the other possible influences. One question that arises is whether these influences are inherently weak (if statistically significant) or if we only believe they must be weak because previous analyses have, for the most part, mistaken time series behavior ("noise") as signal. If it is the former, it is possible that we are measuring the wrong variables in this system and further work should be done to identify currently unmeasured influences. If the latter, we must be satisfied with the explanation that this is a very noisy system. Much of the problem here, unfortunately, is that we can only observe what happens and are unable to experimentally manipulate levels of possible drivers to measure their effects. A randomized application of experimental treatments would allow us to minimize spurious correlations and draw firmer conclusions that correlated parameters are causative drivers and not merely associated, but this is obviously not achievable.

7. Conclusions

1. Although electron fluxes (20 eV–2 MeV) from the RBSP-B satellite are correlated with solar wind and IMF variables, the SME index (substorms), ULF waves, and geomagnetic indices over L-shells 2–6, removing correlation-inflating common cycles and trends (using autoregressive and moving average terms in an ARMAX analysis) results in a roughly 10 times reduction in apparent association between these variables and electron flux. While lower, many are still statistically significant ($p < 0.05$), with the most influence seen in the 20 eV–1 keV and 1–2 MeV electrons. More modest associations are seen in the midrange energies (2–40 keV).
2. Solar wind velocity and pressure (but not number density), IMF magnitude (with lower influence of B_z), SME (a substorm measure), a ULF wave index, and geomagnetic indices Kp and SymH show associations with electron flux in the ARMAX individual analyses which are corrected for time series behavior.
3. We postulate that only substorms (electron injection), ULF waves (radial diffusion), and pressure (magnetosphere compression and/or magnetopause shadowing) are direct drivers of electron flux. We compare their influences in a combined analysis. This essentially studies each variable with the others held constant. SME is the strongest influence of these three, mainly in the MeV and eV electrons. ULF waves are most influential at the highest (1–2 MeV) energies. Pressure is less associated with flux, and there is only a suggestion of possible compression or magnetopause shadowing in the first minutes (L-shell 2) or within 1–2 hr (L-shell 3–5) at the lowest energy. However, we have not ruled out the possibility that this negative influence is due merely to the compression of the magnetosphere below the nominal L-shell (Although chorus waves may be a driver as well, we do not have the data to study this question here.)
4. Predictive models may improve forecasting ability by including indirect driver and proxy parameters, and may, for efficiency, not explictly model time series behavior. However, in order to draw valid conclusions about physical influences of exogenous parameters, we must correct for the autocorrelation and cycling behavior as we do in this present study.

Data Availability Statement

OMNIWeb data is available at https://omniweb.gsfc.nasa.gov/form/dx1.html, the SuperMAG SME and SMEd indices at https://supermag.jhuapl.edu/, the ULF index at http://ulf.gcras.ru/archive.html and the omnidirectional, pitch-angle-resolved flux from RBSP at https://rbsp-ect.newmexicoconsortium.org/datapub/rbspa/ECT/level3/ within https://rbsp-ect.newmexicoconsortium.org/science/DataDirectories.php.

Acknowledgments
The work at the University of Michigan was partly funded by National Aeronautics and Space Administration Grant 80NSSC20K0353 and National Science Foundation Grants 1663770 and 2246912. We thank H. Funsten, J. Blake, D. Baker, and H. Spence for processing and analysis of the HOPE, MagEIS, REPT, and ECT data supported by Energetic Particle, Composition, and Thermal Plasma (RBSP-ECT) investigation funded under NASA's Prime contract no. NAS5-01072. All RBSP-ECT data are publicly available at the Web site http://www.RBSP-ect.lanl.gov/. We gratefully acknowledge the SuperMAG collaborators (https://supermag.jhuapl.edu/info/?page=acknowledgement) for the SME index data, and two anonymous reviewers whose thoughtful comments improved this work.

References

Baker, D. N., Kanekal, S. G., Hoxie, V. C., Batiste, S., Bolton, M., Li, X., et al. (2012). The Relativistic Electron-Proton Telescope (REPT) instrument on board the Radiation Belt Storm Probes (RBSP) spacecraft: Characterization of earth's radiation belt high-energy particle populations. *Space Science Reviews*, *179*(1–4), 1–4. https://doi.org/10.1007/s11214-012-9950-9

Balikhin, M. A., Boynton, R. J., Walker, S. N., Borovsky, J. E., Billings, S. A., & Wei, H. L. (2011). Using the NARMAX approach to model the evolution of energetic electrons fluxes at geostationary orbit. *Geophysical Research Letters*, *38*(18). https://doi.org/10.1029/2011GL048980

Balikhin, M. A., Rodriguez, J. B., Walker, S., Aryan, H., Sibeck, D., & Billings, S. (2016). Comparative analysis of NOAA REFM and SNB3GEO tools for the forecast of the fluxes of high-energy electrons at GEO. *Space Weather*, *14*(1), 22–31. https://doi.org/10.1002/2015SW001303

Birn, J., Thomsen, M. F., Borovsky, J. E., Reeves, G. D., McComas, D. J., & Belian, R. D. (1997). Characteristic plasma properties of dispersionless substorm injections at geosynchronous orbit. *Journal of Geophysical Research*, *102*, 2309. https://doi.org/10.1029/96JA02870

Blake, J. B., Carranza, P. A., Claudepierre, S. G., Clemmons, J. H., Jr., Dotan, Y., Zakrzewski, M. P., et al. (2013). The Magnetic Electron Ion Spectrometer (MagEIS) instruments aboard the Radiation Belt Storm Probes (RBSP) spacecraft. *Space Science Reviews*, *179*(1–4), 1–4. https://doi.org/10.1007/S11214-013-9991-8

Borovsky, J. E., & Denton, M. H. (2014). Exploring the cross correlations and autocorrelations of the ULF indices and incorporating the ULF indices into the systems science of the solar wind-driven magnetosphere. *Journal of Geophysical Research: Space Physics*, *119*(6), 4307–4334. https://doi.org/10.1002/2014JA019876

Boyd, A. J., Spence, H. E., Claudepierre, S. G., Fennell, J. F., Blake, J. B., Baker, D. N., et al. (2014). Quantifying the radiation belt seed population in the 17 March 2013 electron acceleration event. *Geophysical Research Letters*, *41*(7), 2275–2281. https://doi.org/10.1002/2014GL059626

Boyd, A. J., Spence, H. E., Reeves, G. D., Funsten, H. O., Skoug, R. M., Larsen, B. A., et al. (2021). RBSP-ECT combined pitch angle resolved electron flux data product. *Journal of Geophysical Research: Space Physics*, *126*(3), e2020JA028637. https://doi.org/10.1029/2020JA028637

Boynton, R. J., Balikhin, M. A., & Billings, S. A. (2015). Online NARMAX model for electron fluxes at GEO. *Annales Geophysicae*, *33*(3), 405–411. https://doi.org/10.5194/angeo-33-405-2015

Boynton, R. J., Balikhin, M. A., Billings, S. A., Reeves, G. D., Ganushkina, N., Gedalin, M., et al. (2013). The analysis of electron fluxes at geosynchronous orbit employing a NARMAX approach. *Journal of Geophysical Research: Space Physics*, *118*(4), 1500–1513. https://doi.org/10.1002/jgra.50192

Boynton, R. J., Balikhin, M. A., Billings, S. A., Wei, H. L., & Ganushkina, N. (2011). Using the NARMAX OLS-ERR algorithm to obtain the most influential coupling functions that affect the evolution of the magnetosphere. *Journal of Geophysical Research*, *116*(A5). https://doi.org/10.1029/2010JA015505

Denton, M. H., Henderson, M. G., Jordanova, V. K., Thomsen, M. F., Borovsky, J. E., Woodroffe, J., et al. (2016). An improved empirical model of electron and ion fluxes at geosynchronous orbit based on upstream solar wind conditions. *Space Weather*, *14*(7), 511–523. https://doi.org/10.1002/2016SW001409

Dubyagin, S., Ganushkina, N. Y., Sillanpää, I., & Runov, A. (2016). Solar wind-driven variations of electron plasma sheet densities and temperatures beyond geostationary orbit during storm times. *Journal of Geophysical Research: Space Physics*, *121*(9), 8343–8360. https://doi.org/10.1002/2016JA022947

Friedel, R., Reeves, G., & Obara, T. (2002). Relativistic electron dynamics in the inner magnetosphere — A review. *Journal of Atmospheric and Solar-Terrestrial Physics*, *64*(2), 265–282. https://doi.org/10.1016/S1364-6826(01)00088-8

Funsten, H. O., Skoug, R. M., Guthrie, A. A., MacDonald, E. A., Baldonado, J. R., Harper, R. W., et al. (2013). Helium, Oxygen, Proton, and Electron (HOPE) mass spectrometer for the radiation belt storm probes mission. *Space Science Reviews*, *179*(1–4), 1–4. https://doi.org/10.1007/s11214-013-9968-7

Ganushkina, N. Y., Sillanpää, I., Welling, D., Haiducek, J., Liemohn, M., Dubyagin, S., & Rodriguez, J. V. (2019). Validation of Inner Magnetosphere Particle Transport and Acceleration Model (IMPTAM) with long-term GOES MAGED measurements of keV electron fluxes at geostationary orbit. *Space Weather*, *17*(5), 687–708. https://doi.org/10.1029/2018SW002028

Ganushkina, N. Y., Swiger, B., Dubyagin, S., Matéo-Vélez, J.-C., Liemohn, M. W., Sicard, A., & Payan, D. (2021). Worst-case severe environments for surface charging observed at LANL satellites as dependent on solar wind and geomagnetic conditions. *Space Weather*, *19*(9), e2021SW002732. https://doi.org/10.1029/2021SW002732

Gjerloev, J. W. (2012). The SuperMAG data processing technique. *Journal of Geophysical Research*, *117*(A9), A09213. https://doi.org/10.1029/2012JA017683

Hao, Y. X., Zong, Q.-G., Zhou, X.-Z., Rankin, R., Chen, X. R., Liu, Y., et al. (2019). Global-scale ULF waves associated with SSC accelerate magnetospheric ultrarelativistic electrons. *Journal of Geophysical Research: Space Physics*, *124*(3), 1525–1538. https://doi.org/10.1029/2018JA026134

Hartley, D. P., Denton, M. H., & Rodriguez, J. V. (2014). Electron number density, temperature, and energy density at GEO and links to the solar wind: A simple predictive capability. *Journal of Geophysical Research: Space Physics*, *119*(6), 4556–4571. https://doi.org/10.1002/2014JA019779

Hwang, J. A., Lee, D.-Y., Lyons, L. R., Smith, A. J., Zou, S., Min, K. W., et al. (2007). Statistical significance of association between whistler-mode chorus enhancements and enhanced convection periods during highspeed streams. *Journal of Geophysical Research*, *112*, A09213. https://doi.org/10.1029/2007JA012388

Hyndman, R., & Athanasopoulos, G. (2018). *Forecasting: Principles and practice*. Heathmont, OTexts.

Jaynes, A. N., Baker, D. N., Singer, H. J., Rodriguez, J. V., Loto'aniu, T. M., Ali, A. F., et al. (2015). Source and seed populations for relativistic electrons: Their roles in radiation belt changes. *Journal of Geophysical Research: Space Physics*, *120*(9), 7240–7254. https://doi.org/10.1002/2015JA021234

Katsavrias, C., Daglis, I. A., Li, W., Dimitrakoudis, S., Georgiou, M., Turner, D. L., & Papadimitriou, C. (2015). Combined effects of concurrent Pc5 and chorus waves on relativistic electron dynamics. *Annales Geophysicae*, *33*(9), 1173–1181. https://doi.org/10.5194/angeo-33-1173-2015

Katsavrias, C., Sandberg, I., Li, W., Podladchikova, O., Daglis, I. A., Papadimitriou, C., et al. (2019). Highly relativistic electron flux enhancement during the weak geomagnetic storm of April–May 2017. *Journal of Geophysical Research: Space Physics*, *124*(6), 4402–4413. https://doi.org/10.1029/2019JA026743

Kellerman, A. C., & Shprits, Y. Y. (2012). On the influence of solar wind conditions on the outer-electron radiation belt. *Journal of Geophysical Research*, *117*(A5). https://doi.org/10.1029/2011JA017253

Kozyreva, O., Pilipenko, V., Engebretson, M., Yumoto, K., Watermann, J., & Romanova, N. (2007). In search of a new ULF wave index: Comparison of Pc5 power with dynamics of geostationary relativistic electrons. *Planetary and Space Science*, *55*(6), 755–769. https://doi.org/10.1016/j.pss.2006.03.013

Lam, H.-L. (2004). On the prediction of relativistic electron fluence based on its relationship with geomagnetic activity over a solar cycle. *Journal of Atmospheric and Solar-Terrestrial Physics*, *66*(18), 1703–1714. https://doi.org/10.1016/j.jastp.2004.08.002

Lam, H.-L., Boteler, D. H., Burlton, B., & Evans, J. (2012). Anik-E1 and E2 satellite failures of January 1994 revisited. *Space Weather*, *10*(10). https://doi.org/10.1029/2012SW000811

Lejosne, S. (2020). Electromagnetic radial diffusion in the earth's radiation belts as determined by the solar wind immediate time history and a toy model for the electromagnetic fields. *Journal of Geophysical Research: Space Physics*, *125*(6), e2020JA027893. https://doi.org/10.1029/2020JA027893

Li, X., Baker, D. N., Temerin, M., Reeves, G., Friedel, R., & Shen, C. (2005). Energetic electrons, 50 keV to 6 MeV, at geosynchronous orbit: Their responses to solar wind variations. *Space Weather*, *3*(4). https://doi.org/10.1029/2004SW000105

Li, X., Temerin, M., Baker, D. N., Reeves, G. D., & Larson, D. (2001). Quantitative prediction of radiation belt electrons at geostationary orbit based on solar wind measurements. *Geophysical Research Letters*, *28*(9), 1887–1890. https://doi.org/10.1029/2000GL012681

Loto'aniu, T. M., Singer, H. J., Rodriguez, J. V., Green, J., Denig, W., Biesecker, D., & Angelopoulos, V. (2015). Space weather conditions during the Galaxy 15 spacecraft anomaly. *Space Weather*, *13*(8), 484–502. https://doi.org/10.1002/2015SW001239

Loto'aniu, T. M., Singer, H. J., Waters, C. L., Angelopoulos, V., Mann, I. R., Elkington, S. R., & Bonnell, J. W. (2010). Relativistic electron loss due to ultralow frequency waves and enhanced outward radial diffusion. *Journal of Geophysical Research*, *115*(A12245). https://doi.org/10.1029/2010JA015755

Luo, B., Tu, W., Li, X., Gong, J., Liu, S., Burin des Roziers, E., & Baker, D. N. (2011). On energetic electrons (>38*kev*) in the central plasma sheet: Data analysis and modeling. *Journal of Geophysical Research*, *116*(A9), A09220. https://doi.org/10.1029/2011ja016562

Lyatsky, W., & Khazanov, G. V. (2008). Effect of solar wind density on relativistic electrons at geosynchronous orbit. *Geophysical Research Letters*, *35*(3). https://doi.org/10.1029/2007GL032524

Ma, D., Bortnik, J., Chu, X., Claudepierre, S. G., Ma, Q., & Kellerman, A. (2023). Opening the black box of the radiation belt machine learning model. *Space Weather*, *21*(4), e2022SW003339. https://doi.org/10.1029/2022SW003339

Mann, I., O'Brien, T., & Milling, D. (2004). Correlations between ULF wave power, solar wind speed, and relativistic electron in the magnetosphere: Solar cycle dependence. *Journal of Atmospheric and Solar-Terrestrial Physics*, *66*(2), 187–198. https://doi.org/10.1016/j.jastp.2003.10.002

Mann, K. R., Murphy, I. R., Ozeke, L. G., Rae, I., Milling, D. K., Kale, A., & Honary, F. F. (2012). The role of ultralow frequency waves in radiation belt dynamics. *Geographical Monograph Series*, *199*, 69–92. https://doi.org/10.1029/2012GM001349

Matéo-Vélez, J.-C., Sicard, A., Payan, D., Ganushkina, N., Meredith, N. P., & Sillanpää, I. (2018). Spacecraft surface charging induced by severe environments at geosynchronous orbit. *Space Weather*, *16*(1), 89–106. https://doi.org/10.1002/2017SW001689

Mauk, B., Fox, N., Kanekal, S., Kessel, R., Sibeck, D., & Ukhorskiy, A. (2013). Science objectives and rationale for the radiation belt storm probes mission. *Space Science Reviews*, *179*(1–4), 3–27. https://doi.org/10.1007/s11214-012-9908-y

Neter, J., Kutner, M. H., & Wassermann, W. (1990). *Applied linear statistical models* (3rd ed.). Irwin.

Newell, P., & Gjerloev, J. W. (2011). Evaluation of SuperMAG auroral electrojet indices as indicators of substorms and auroral power. *Journal of Geophysical Research*, *116*(A12), A12211. https://doi.org/10.1029/2011JA016779

O'Brien, T. P., & McPherron, R. L. (2003). An empirical dynamic equation for energetic electrons at geosynchronous orbit. *Journal of Geophysical Research*, *108*(A3), 1137. https://doi.org/10.1029/2002JA009324

Ozeke, L. G., Mann, I. R., Dufresne, S. K. Y., Olifer, L., Morley, S. K., Claudepierre, S. G., et al. (2020). Rapid outer radiation belt flux dropouts and fast acceleration during the March 2015 and 2013 storms: The role of ULF wave transport from a dynamic outer boundary. *Journal of Geophysical Research: Space Physics*, *125*(2), e2019JA027179. https://doi.org/10.1029/2019JA027179

Ozeke, L. G., Mann, I. R., Murphy, K. R., Rae, I. J., & Milling, D. K. (2014). Analytic expressions for ULF wave radiation belt radial diffusion coefficients. *Journal of Geophysical Research: Space Physics*, *119*(3), 1587–1605. https://doi.org/10.1002/2013JA019204

Paulikas, G., & Blake, J. (1979). Effects of the solar wind on magnetospheric dynamics: Energetic electrons at the synchronous orbit. In *Quantitative modeling of magnetospheric processes* (pp. 180–202). American Geophysical Union (AGU). https://doi.org/10.1029/GM021p0180

Romanova, N., & Pilipenko, V. (2009). ULF wave indices to characterize the solar wind-magnetosphere interaction and relativistic electron dynamics. *Acta Geophysica*, *57*(1), 158–170. https://doi.org/10.2478/s11600-008-0064-4

Sakaguchi, K., Miyoshi, Y., Saito, S., Nagatsuma, T., Seki, K., & Murata, K. T. (2013). Relativistic electron flux forecast at geostationary orbit using Kalman filter based on multivariate autoregressive model. *Space Weather*, *11*(2), 79–89. https://doi.org/10.1002/swe.20020

Sakaguchi, K., Nagatsuma, T., Reeves, G. D., & Spence, H. E. (2015). Prediction of MeV electron fluxes throughout the outer radiation belt using multivariate autoregressive models. *Space Weather*, *13*(12), 853–867. https://doi.org/10.1002/2015SW001254

Shi, Y., Zesta, E., & Lyons, L. R. (2009). Features of energetic particle radial profiles inferred from geosynchronous responses to solar wind dynamic pressure enhancements. *Annales Geophysicae*, *27*(2), 851–859. https://doi.org/10.5194/angeo-27-851-2009

Shprits, Y. Y., Thorne, R. M., Friedel, R., Reeves, G. D., Fennell, J., Baker, D. N., & Kanekal, S. G. (2006). Outward radial diffusion driven by losses at magnetopause. *Journal of Geophysical Research*, *111*(A11214). https://doi.org/10.1029/2006JA011657

Sillanpää, I., Ganushkina, N. Y., Dubyagin, S., & Rodriguez, J. V. (2017). Electron fluxes at geostationary orbit from GOES MAGED data. *Space Weather*, *15*(12), 1602–1614. https://doi.org/10.1002/2017SW001698

Simms, L. E., & Engebretson, M. (2020). Classifier neural network models predict relativistic electron events at geosynchronous orbit better than multiple regression or ARMAX models. *Journal of Geophysical Research: Space Physics*, *125*(5), e2019JA027357. https://doi.org/10.1029/2019JA027357

Simms, L. E., Engebretson, M., Clilverd, M., Rodger, C., Lessard, M., Gjerloev, J., & Reeves, G. (2018). A distributed lag autoregressive model of geostationary relativistic electron fluxes: Comparing the influences of waves, seed and source electrons, and solar wind inputs. *Journal of Geophysical Research: Space Physics*, *123*(5), 3646–3671. https://doi.org/10.1029/2017JA025002

Simms, L. E., Engebretson, M., & Reeves, G. (2022). Removing diurnal signals and longer term trends from electron flux and ULF correlations: A comparison of spectral subtraction, simple differencing, and ARIMAX models. *Journal of Geophysical Research*, *127*(2), e2021JA030021. https://doi.org/10.1029/2021JA030021

Simms, L. E., Engebretson, M. J., Clilverd, M. A., Rodger, C. J., & Reeves, G. D. (2018). Nonlinear and synergistic effects of ULF Pc5, VLF Chorus, and EMIC waves on relativistic electron flux at geosynchronous orbit. *Journal of Geophysical Research: Space Physics*, *123*(6), 4755–4766. https://doi.org/10.1029/2017JA025003

Simms, L. E., Engebretson, M. J., Pilipenko, V., Reeves, G. D., & Clilverd, M. (2016). Empirical predictive models of daily relativistic electron flux at geostationary orbit: Multiple regression analysis. *Journal of Geophysical Research: Space Physics*, *121*(4), 3181–3197. https://doi.org/10.1002/2016JA022414

Simms, L. E., Engebretson, M. J., & Reeves, G. D. (2023). Determining the timing of driver influences on 1.8–3.5 MeV electron flux at geosynchronous orbit using ARMAX methodology and stepwise regression. *Journal of Geophysical Research: Space Physics*, *128*(1), e2022JA030963. https://doi.org/10.1029/2022JA030963

Simms, L. E., Engebretson, M. J., Rodger, C. J., Dimitrakoudis, S., Mann, I. R., & Chi, P. J. (2021). The combined influence of lower band chorus and ULF waves on radiation belt electron fluxes at individual L-shells. *Journal of Geophysical Research: Space Physics*, *126*(5), e2020JA028755. https://doi.org/10.1029/2020JA028755

Simms, L. E., Engebretson, M. J., Rodger, C. J., Gjerloev, J. W., & Reeves, G. D. (2019). Predicting lower band chorus with autoregressive-moving average transfer function (ARMAX) models. *Journal of Geophysical Research: Space Physics*, *124*(7), 5692–5708. https://doi.org/10.1029/2019JA026726

Simms, L. E., Ganushkina, N. Y., der Kamp, M. V., Balikhin, M., & Liemohn, M. W. (2023). Predicting geostationary 40-150 keV electron flux using ARMAX (an autoregressive moving average transfer function), RNN (a recurrent neural network), and logistic regression: A comparison of models. *Space Weather*, *21*(5), e2022SW003263. https://doi.org/10.1029/2022SW003263

Simms, L. E., Ganushkina, N. Y., van de Kamp, M., Liemohn, M. W., & Dubyagin, S. (2022). Using ARMAX models to determine the drivers of 40-150 keV GOES electron fluxes. *Journal of Geophysical Research*, *127*(9), e2022JA030538. https://doi.org/10.1029/2022JA030538

Simms, L. E., Pilipenko, V., Engebretson, M. J., Reeves, G. D., Smith, A. J., & Clilverd, M. (2014). Prediction of relativistic electron flux at geostationary orbit following storms: Multiple regression analysis. *Journal of Geophysical Research: Space Physics*, *119*(9), 7297–7318. https://doi.org/10.1002/2014JA019955

Spence, H. E., Reeves, G. D., Baker, D. N., Blake, J. B., Bolton, M., Bourdarie, S., et al. (2013). Science goals and overview of the Radiation Belt Storm Probes (RBSP) energetic particle, composition, and thermal plasma (ECT) suite on NASA's van allen probes mission. *Space Science Reviews*, *179*(1–4), 1–4. https://doi.org/10.1007/s11214-013-0007-5

Staples, F. A., Kellerman, A., Murphy, K., Rae, I. J., Sandhu, J. K., & Forsyth, C. (2022). Resolving magnetopause shadowing using multimission measurements of phase space density. *Journal of Geophysical Research: Space Physics*, *127*(2), e2021JA029298. https://doi.org/10.1029/2021JA029298

Stepanov, N. A., Sergeev, V. A., Sormakov, D. A., Andreeva, V. A., Dubyagin, S. V., Ganushkina, N., et al. (2021). Superthermal proton and electron fluxes in the plasma sheet transition region and their dependence on solar wind parameters). *journal = Journal of Geophysical Research: Space Physics, volume =*, *126*(4), e2020JA028580. https://doi.org/10.1029/2020JA028580

Su, Y.-J., Quinn, J. M., Johnston, W. R., McCollough, J. P., & Starks, M. J. (2014). Specification of > 2 MeV electron flux as a function of local time and geomagnetic activity at geosynchronous orbit. *Space Weather*, *12*(7), 470–486. https://doi.org/10.1002/2014SW001069

Summers, D., Ma, C., Meredith, N. P., Horne, R. B., Thorne, R. M., Heynderickx, D., & Anderson, R. R. (2002). Model of the energization of outer-zone electrons by whistler-mode chorus during the October 9, 1990 geomagnetic storm. *Geophysical Research Letters*, *29*(24), 2174. https://doi.org/10.1029/2002GL016039

Swiger, B. M., Liemohn, M. W., Ganushkina, N. Y., & Dubyagin, S. (2022). Energetic electron flux predictions in the near-earth plasma sheet from solar wind driving. *Space Weather*, *20*(11), e2022SW003150. https://doi.org/10.1029/2022SW003150

The MathWorks Inc. (2023). MATLAB version: 23.2.0 (R2023b). The MathWorks Inc. Retrieved from https://www.mathworks.com

Thomsen, M. F., Henderson, M. G., & Jordanova, V. K. (2013). Statistical properties of the surface-charging environment at geosynchronous orbit. *Space Weather*, *11*(5), 237–244. https://doi.org/10.1002/swe.20049

Tu, W., Xiang, Z., & Morley, S. K. (2019). Modeling the magnetopause shadowing loss during the June 2015 dropout event. *Geophysical Research Letters*, *46*(16), 9388–9396. https://doi.org/10.1029/2019GL084419

Turner, D. L., Shprits, Y., Hartinger, M., & Angelopoulos, V. (2012). Explaining sudden losses of outer radiation belt electrons during geomagnetic storms. *Nature Physics Letters*, *8*(3), 208–212. https://doi.org/10.1038/NPHYS2185